Effect of Blade Number on a Straight-Bladed Vertical-Axis Darreius Wind Turbine

Marco Raciti Castelli, Stefano De Betta and Ernesto Benini

***Abstract*—**This paper presents a mean for reducing the torque variation during the revolution of a vertical-axis wind turbine (VAWT) by increasing the blade number. For this purpose, two-dimensional CDF analysis have been performed on a straight-bladed Darreius-type rotor. After describing the computational model, a complete campaign of simulations based on full RANS unsteady calculations is proposed for a three, four and five-bladed rotor architecture characterized by a NACA 0025 airfoil. For each proposed rotor configuration, flow field characteristics are investigated at several values of tip speed ratio, allowing a quantification of the influence of blade number on flow geometric features and dynamic quantities, such as rotor torque and power. Finally, torque and power curves are compared for the analyzed architectures, achieving a quantification of the effect of blade number on overall rotor performance.

***Keywords*—**CFD, VAWT, NACA 0021, blade number

I. Introduction and Background

EUROPE gets approximately 20% of its electricity from renewable energy sources, including 5.3% from wind Energy. That share will increase up to 2020 when, under the terms of the EU's renewable energy directive, which sets legally binding targets for renewable energy in Europe, 34% of the EU's total electricity consumption will come from renewable energy sources, with wind energy accounting for 14% [1]. In this scenario, the research in wind energy systems acquires considerable importance.

This continuous quest for clean energy is now focusing on the local production of electric power, spread in a wide area, so as to cooperate with the big electric power plants located in just few specific strategic locations of the countries. One of the most promising resources is wind power associated with local production of clean electric power inside the built environment, such as industrial and residential areas, which has lead to the development of the so called computational wind engineering. The new discipline has also renewed the interest in vertical axis wind turbines (VAWTs) [2].

The differences between an horizontal and a vertical axis wind turbine are many, including their utilization: horizontal axis wind turbine is popular for large scale power generation, while the vertical axis wind turbine is utilized for small scale power generation [3,4].

Many factors play a role in the design of a wind turbine rotor, including aerodynamics, generator characteristics, blade strength and rigidity, noise levels. But since a small wind energy conversion system's success is largely dependent on maximizing its energy extraction, rotor aerodynamics play a critical role in the minimization of the cost of energy [5]. A widely used way to improve the aerodynamics of wind turbines is the utilization of computational fluid dynamics (CFD), which is less expensive than experimental tests and saves a lot of time and work. Also it permits the knowledge of the entire flow field.

As pointed out by Ferreira [6], the VAWT has an inherent unsteady aerodynamic behavior due to the variation of the angle of attack with the azimuthal position, of the relative velocity and, consequentially, of the Reynolds number. The phenomenon of dynamic stall is then an intrinsic effect of the operation of this kind of turbine, having a significant impact in loads and power. The complexity of the unsteady aerodynamics of a VAWT requires an accurate selection of the appropriate turbulence model and Ferreira demonstrated that the *Detached Eddy Simulation* model provides a good prediction of dynamic stall development, even for 2D computations.

Wang and Tao [7] performed numerical simulations using RANS model, by solving the Navier-Stokes equations with two low Reynolds number turbulence models. They compared the SST k-ω model with low Reynolds number correction and the v^2-f model to simulate the fluid flow field around a pitching NACA 0012. The conclusion was that both the two turbulence models can predict the experimental data with reasonable accuracy, except at very high angles of attack where the flow is fully detached. They stated that, in order to obtain a very detailed understanding of the main aspects of the dynamic stall phenomenon, the capability of advanced CFD methods, such as LES of DES, needs to be examined. However the RANS approach is still good for fast design or research of low Reynolds number airfoils, because they are capable of capturing a significant part of the flow dynamics.

Between the many factors that influence the aerodynamic behavior of the rotor, an important role is played by its solidity, defined as:

$$\sigma = N\, c / R_{rotor}. \quad (1)$$

where N is blade number [-], c is blade chord [m] and R is rotor radius [m].

Marco Raciti Castelli is Research Associate at the Department of Mechanical Engineering of the University of Padua, Via Venezia 1, 35131 Padova, Italy (e-mail: marco.raciticastelli@unipd.it).

Stefano De Betta is completing his M.Sc. thesis in Aerospace Engineering at University of Padua, Via Venezia 1, 35131 Padova, Italy.

Ernesto Benini is Associate Professor at the Department of Mechanical Engineering of the University of Padua, Via Venezia 1, 35131 Padova, Italy (e-mail: ernesto.benini@unipd.it).

As pointed out by Howell et al.[8], solidity is one of the main parameters dictating the rotational velocity ay which the turbine reaches its maximum performance coefficient. With experimental studies he compared the behavior of a two and three bladed VAWT, and demonstrated that the two bladed generates an higher power than the three bladed and the peak power is obtained for higher values of tip speed ratio.

Li S., and Li Y. [3] made a series of numerical analysis about the effect of solidity on a straight-bladed VAWT, changing both blade chord and number of blades. They stated that the VAWT with larger solidity achieves maximum power at lower tip speed ratio. However, too large solidity will decrease the power coefficient. Furthermore, even for the same solidity, the different combination of blade number and chord affects the power performance of VAWTs greatly.

In this work, two-dimensional CFD simulations of the flow field around a tree-bladed, four-bladed and five-bladed Darrieus rotor are performed, with the aim of determining the influence of blade number on the performance of the vertical axis wind turbine. The solutions are obtained using unstructured moving grids rotating with the turbine blades. For each configuration, the flow field characteristics are investigated at several value of tip speed ratio, in order to analyze the changes in the behavior of the turbine, due to the variation of blade number.

II. Model Geometry

The aim of the present work is to numerically analyze the aerodynamic behavior of a three, four and five bladed Darreius VAWT operating at different angular velocities, for a constant wind speed of 9 m/s. The main features of the turbine are summarized in table 1.

TABLE I
MAIN GEOMETRICAL FEATURES OF THE TESTED MODEL

D_{rotor} [mm]	1030
H_{rotor}	1 (2D simulation)
Blade profile	NACA 0025
c [mm]	85.8

The solidity parameter σ is defined as c N / R_{rotor} as suggested by Strickland [9]. For a three, four and five bladed rotor, its values are respectively 0.5, 0.67 and 0.83.

Rotor azimuthal position was identified by the angular coordinate of the pressure centre of blade No. 1 (set at 0.25c for NACA 0025 airfoil), starting between the 2nd and 3rd Cartesian plane octants, as can be seen from Fig.1.

III. Description of the Numerical Flow Field

As the aim of the present work was to reproduce the operation of a rotating machine, the use of moving sub-grids was necessary. In particular, the discretization of the computational domain into macro-areas led to two distinct sub-grids:

- a rectangular outer zone, determining the overall calculation domain, with a circular opening centered on the turbine rotational axis, which was identified as *Wind Tunnel sub-grid*, fixed;
- a circular inner zone, which was identified as *Rotor sub-grid*, rotating with rotor angular velocity ω.

Fig. 2 shows the main dimensions of the *Wind tunnel sub-grid* area.

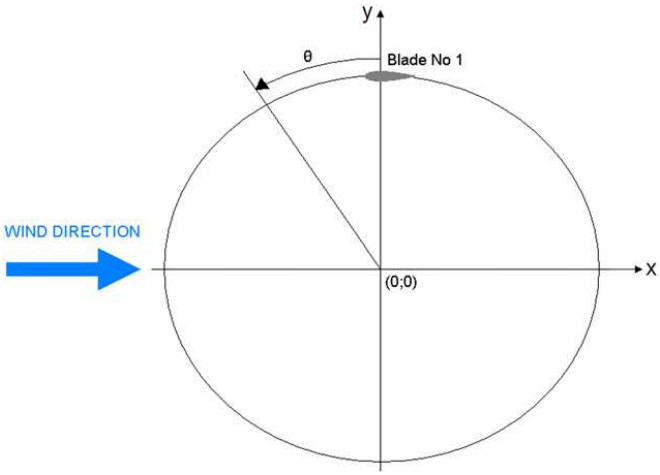

Fig.1 Azimuthal coordinate of blade mid section's centre of pressure

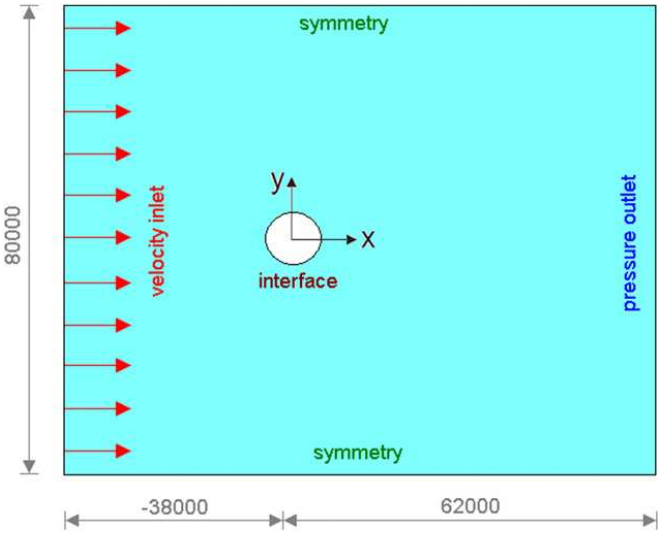

Fig. 2 Main dimensions [mm] of the Wind Tunnel sub-grid area

In order to allow a full development of the wake, Ferreira et al. [6] placed inlet and outlet boundary conditions respectively 10 diameters upwind and 14 diameters downwind with respect to rotor test section for a wind tunnel CFD simulation. As the aim of the present work is the simulation of a turbine operating in open field conditions and because of the huge domain width necessary to avoid solid blockage, inlet and outlet were placed respectively 37 rotor diameters upwind and 60 rotor diameters downwind with respect to the rotor test section.

Inlet was set as a *velocity inlet*, with a constant velocity profile of 9 m/s, while outlet was set as a *pressure outlet*. Two *symmetry* boundary conditions were used for the two side walls. The circumference around the circular opening, centered

on the turbine rotational axis, was set as an *interface*, thus ensuring the continuity in the flow field.

The *Rotor sub-grid* is the fluid area simulating the revolution of the wind turbine and is therefore characterized by a moving mesh, rotating at the same angular velocity of the turbine. Its location coincides exactly with the circular opening inside the *Wind Tunnel sub-grid* area and is centered on the turbine rotational axis. Fig. 3 shows the main dimensions and the boundary conditions of the *Rotor sub-grid* area.

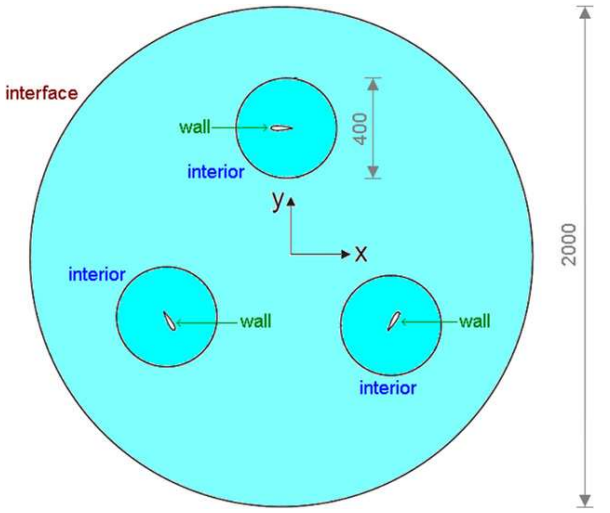

Fig. 3 Schema of rotor sub-grid area for the three bladed VAWT (dimensions in mm)

All blade profiles inside the *Rotor sub-grid* area were enclosed in a control circle of 400 mm diameter. Unlike the interface, it had no physical significance: its aim was to allow a precise dimensional control of the grid elements in the area close to rotor blades, by adopting a first size function operating from the blade profile to the control circle itself and a second size function operating from the control circle to the whole Rotor sub-grid area, ending with grid elements of the same size of the corresponding *Wind tunnel sub grid* elements. An *interior* boundary condition was used for control circle borders, thus ensuring the continuity of the cells on both sides of the mesh.

IV. Discretization of the Numerical Flow Field

As rotating mesh was utilized in order to represent the rotational motion of the VAWT. To discretize the flow field, an unstructured grid was chosen for the entire domain, in order to reduce the engineering time to prepare the CFD simulations. The mesh on both sides of the *interface* (*Rotor sub-grid* and *Wind Tunnel sub-grid* areas) had approximately the same characteristic cell size in order to obtain faster convergence [10].

An isotropic unstructured mesh was chosen for the *Rotor sub-grid*, in order to guarantee the same accuracy in the prediction of rotor's performance during the revolution of the turbine (according to the studies of Commings et al. [11]) and also in order to test the prediction capability of a very simple grid. Considering their features of flexibility and adaption capability, unstructured meshes are in fact very easy to obtain, for complex geometries, too, and often represent the "first attempt" in order to get a quick response from the CFD in engineering work . The Rotor sub-grid mesh is represented in Fig.4 for the four-bladed turbine architecture.

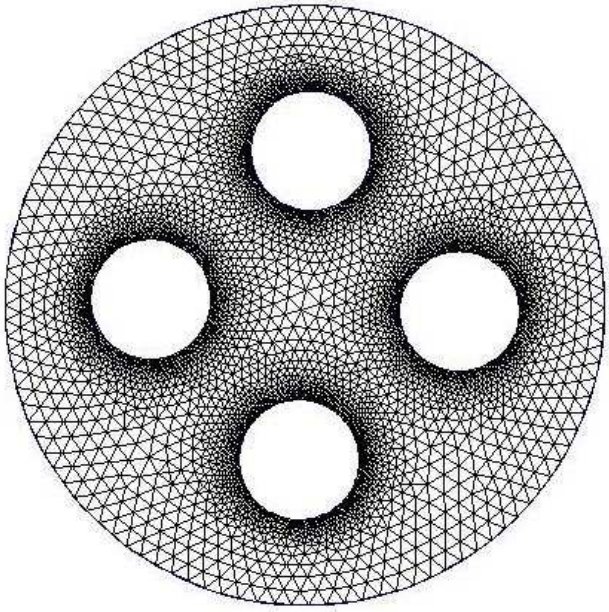

Fig. 4 Rotor sub-grid mesh for the four-bladed VAWT

Being the area close to the blade profiles, great attention was placed in the *control circle*. The computational grids were constructed from lower topologies to higher ones, adopting appropriate size functions, in order to cluster grid points near the leading edge and the trailing edge of the blade profile, so as to improve the CFD code capability of determining lift, drag and the separation of the flow from the blade itself. Table 2 summarizes the main features of the mesh close to rotor blade, while Fig.5 represents the control circle mesh.

TABLE II
Main Features of the Mesh Close to Rotor Blade

Starting grid size from airfoil leading edge [mm]	1.3
Growth factor from airfoil leading edge [-]	1.08
Starting grid size from airfoil trailing edge [mm]	0.4
Growth factor from airfoil trailing edge [-]	1.28
Maximum grid size on airfoil [mm]	3.5
Growth factor from airfoil surface to *Rotor sub-grid* area [mm]	1.25
Maximum grid size on *Rotor sub-grid* area [mm]	10

In order to determine the optimal size of the near wall cells, a statistical analysis of y^+ parameter was performed. For further information about mesh generation and code validation, see [12].

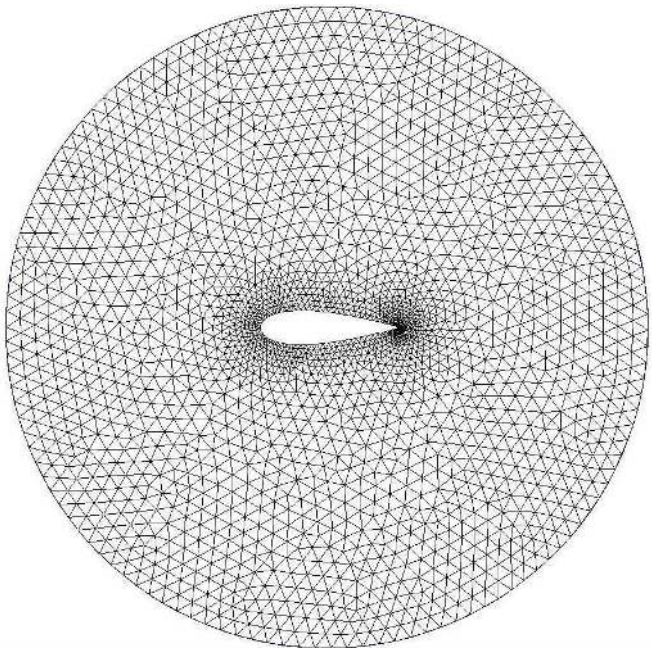

Fig. 5 Control circle grid for NACA 0025 blade section

V. Main Features of the Numerical Simulations

A complete campaign of simulations, based on full RANS unsteady calculations, was performed for a three, four and five-bladed rotor architecture characterized by a NACA 0025 airfoil. The tip speed ratio, defined as:

$$\lambda = \omega R_{rotor} / V_{\infty}. \quad (2)$$

was varied from a value of λ=1.44 (which corresponds to an angular velocity of ω=25.1 rad/s) to λ=3.3 (which corresponds to an angular velocity of ω=57.6 rad/s). These conditions correspond to a range of blade Reynolds numbers from $7.59 \cdot 10^4$ to $1.74 \cdot 10^5$.

The blade Reynolds number for this work was defined as:

$$Re = (R^2 \omega c) / \mu. \quad (3)$$

The dynamic viscosity μ was assumed to be $1.78 \cdot 10^{-5}$ Pa·s, the density ρ was set to 1.225 kg/m^3 and the free stream velocity V_{∞} was set to 9 m/s.

VI. Numerical Solution

As pointed out by McMuller et al. [13], the calculation of unsteady flows in turbomachinery continues to present a severe challenge to CFD. During VAWT operation, the unsteadyness stems mainly from the relative motion of the rotating blade fields and has a fundamental period which depends both on the rate of rotation and on the number of blades. For the proposed calculations, the temporal discretization was achieved by imposing a physical time step equal to the lapse of time the rotor takes to make a 1° rotation.

As a global convergence criterion, each simulation was run until instantaneous torque values showed a deviation of less than 1% compared with the equivalent value of the previous period, for three consecutive periods. The period is a function of the number of blades and corresponds to a revolution of 120°, 90° and 72° respectively for three, four and five blade rotor architecture. Residuals convergence criterion for each physical time step was set to 10^{-5} [14].

As stated by Yu et al. [15], for airfoil flows with great adverse pressure gradient and separation, the choice of a turbulence model is very important. The k-ω SST turbulence model can achieve good results because of its capability of capturing proper behaviour in the near wall layers and separated flow regions. In the case of low Reynolds number, which is typical for wind turbine airfoil flows, laminar-to-turbulent transition is also an important factor that should be taken into account, in order to more accurately predict the flow separation and skin friction.

In the present work, the chosen turbulence model was the k-ω SST, that combines several desirable elements of the existing two-equation models [7].

A 2D pressure based solver was adopted, which is well suited to solve incompressible flows [10]. The unsteady formulation was set to second-order implicit.

VII. Results and Discussion

Fig. 6 represents the evolution of the power coefficient of the three analyzed rotor architectures, defined as:

$$C_p = P/(\tfrac{1}{2} \rho A V_{\infty}^3) \quad (4)$$

as a function of the tip speed ratio, for an incident wind speed of 9 m/s.

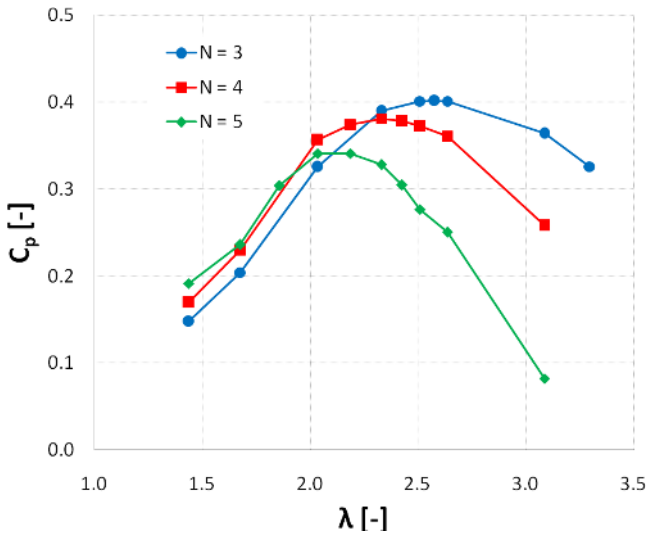

Fig. 6 Power coefficient as a function of tip speed ratio

As can be clearly seen, the peak of power coefficient lowers with the increase of rotor solidity, while it moves to lower tip speed ratio. This means that larger number of blades allow to reach the maximum power coefficient for lower angular speeds, but are penalized as far as efficiency is concerned.

The peak power coefficients for the three analyzed rotor configurations are presented in table 3. Using the power

coefficient of the three-bladed turbine as a reference, a 5% performance decrease is registered for the four-bladed configuration, while the five-bladed architecture exhibits a 15% lowering in the performance. The value of tip speed ratio to obtain the peak power is lowered of 9% for the four-bladed configuration and of 21% for the five-bladed architecture.

TABLE III
VALUES OF PEAK POWER AND CORRESPONDING TIP SPEED RATIOS

	$\lambda_{cp,max}$	$C_{p,max}$
N = 3	2.58	0.40
N = 4	2.33	0.38
N = 5	2.04	0.34

Fig. 7 shows the torque coefficient, defined as:

$$C_t = T/(½ \rho A R_{rotor} V_\infty^2). \quad (5)$$

as a function of the angular position of blade No. 1 (only a single period of revolution is represented for each rotor configuration).

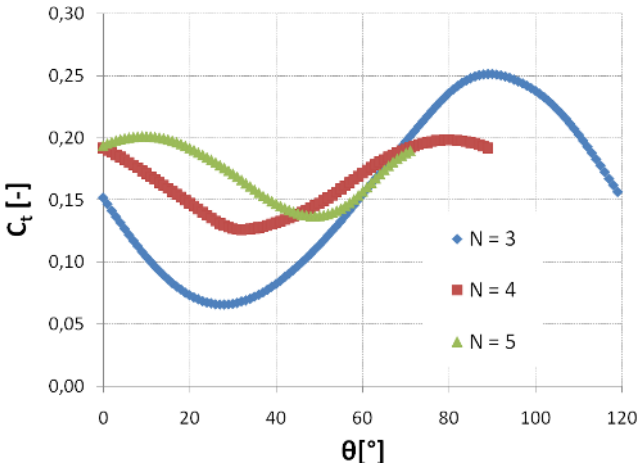

Fig. 7 Torque coefficient as a function of the angular position of blade No. 1 (single period plotted), optimal tip speed ratio (λ=2.58 for N=3, λ=2.33 for N=4, λ=2.04 for N=5)

As can be seen, with the increase of blade number the torque coefficient peak becomes lower and the frequency of the oscillations in the torque is increased. That happens because in a complete 360° rotation of the rotor, the number of periods become higher. The average, maximum and minimum value of Ct for the three analyzed rotors is represented in Table 4, for the tip speed ratio of maximum power coefficient. It can be seen that if the blade number is increased, the oscillations of Ct are reduced, while its average value remain almost constant.

TABLE IV
VALUES OF THE TORQUE COEFFICIENT FOR THE THREE ANALYZED ROTOR CONFIGURATIONS

	$C_{t,avg}$	$C_{t,max}$	$C_{t,min}$
N = 3	0,16	0,25	0,07
N = 4	0,16	0,2	0,12
N = 5	0,17	0,2	0,14

Fig. 8 shows the relation between the azimuthal position and the torque coefficient of blade No. 1. It can be seen that the maximum torque values are generated during the upwind revolution of the turbine and for azimuthal positions where rotor blades are experiencing very high relative angles of attack, even beyond the stall limit, as already observed by Raciti Castelli et al. [14]. The angular position of maximum instantaneous torque coefficient is approximately 90° for all the three cases.

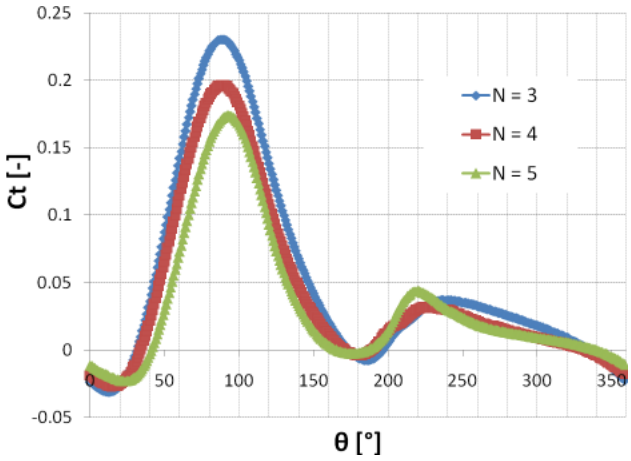

Fig. 8 Istantaneous torque coefficient of a single airfoil as a function of azimuthal coordinate, optimal tip speed ratio (λ=2.58 for N=3, λ=2.33 for N=4, λ=2.04 for N=5)

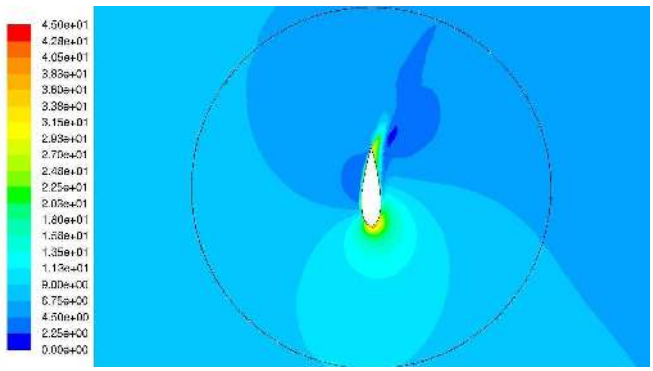

Fig. 9 Contours of absolute velocity [m/s] for the angular position of maximum torque coefficient (θ=90°), N=3, λ=2.58

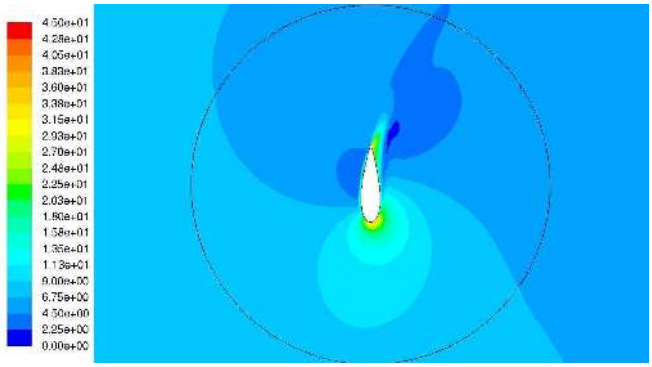

Fig. 10 Contours of absolute velocity [m/s] for the angular position of maximum torque coefficient (θ=90°), N=4, λ=2.33

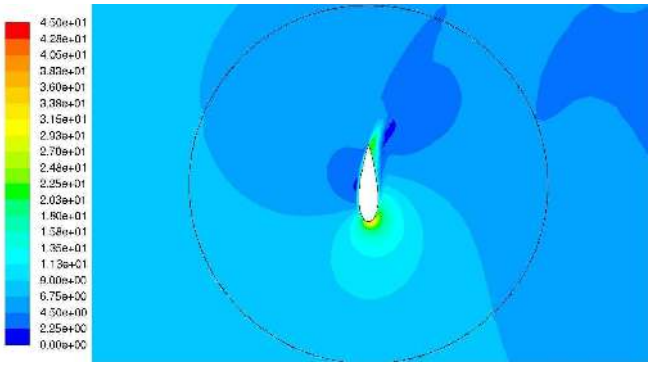

Fig. 11 Contours of absolute velocity [m/s] for the angular position of maximum torque coefficient (θ=90°), N=5, λ=2.04

The contours of absolute velocity around the airfoil, for the point of maximum torque coefficient and for the three analyzed rotor configurations are shown in Figs. 9, 10 and 11. As can be clearly seen, no significant variations are registered.

Figs. 12, 13 and 14 represent the contours of absolute velocity for the whole rotor area. Again, no significant variations are registered, probably due to the fact that the tip speed ratios of optimum power coefficient resulted quite close each other.

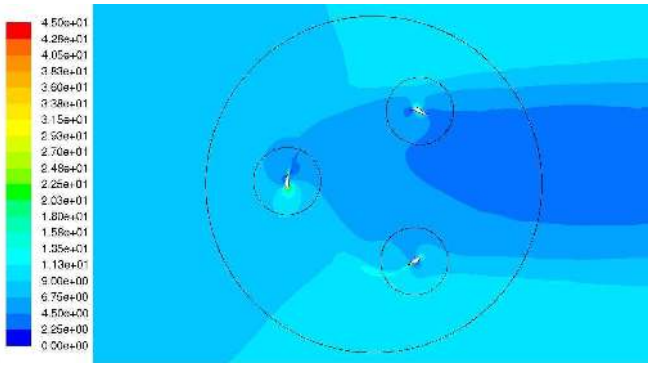

Fig. 12 Contours of absolute velocity [m/s] for the whole rotor for the angular position of maximum torque coefficient (θ= 88°), N=3, λ=2.58

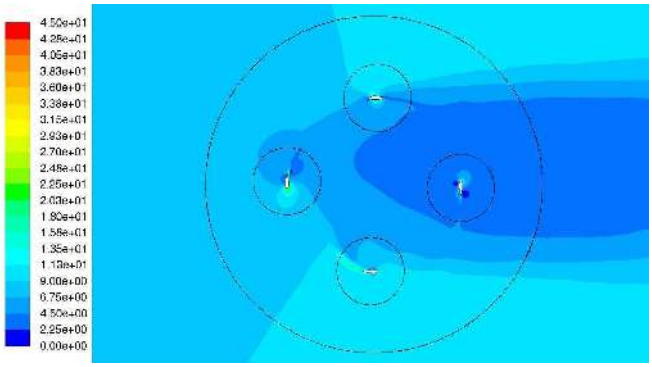

Fig. 13 Contours of absolute velocity [m/s] for the whole rotor for the angular position of maximum torque coefficient (θ= 88°), N=4, λ=2.33

Fig. 15 shows the effect of the increment of blade number on the aerodynamic radial force F_n acting on blade No. 1 over an entire revolution. This component of the resultant force acting on the airfoil does not produce any effect on the torque of the rotor, but its amplitude can cause structural damages. As can be clearly seen, the increment of blade number achieved a reduction of the peak of the radial force. Table 5 presents the values of the maximum radial force and the variation with respect to the force obtained for the three bladed rotor (as the aim of this work is to investigate the effect of the blade number on the aerodynamic of the blade, the centrifugal force has been neglected).

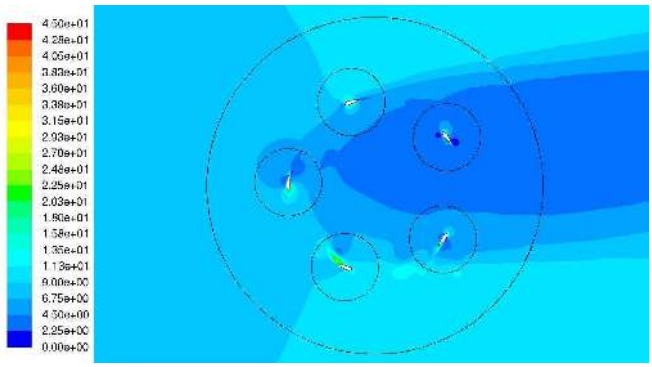

Fig. 14 Contours of absolute velocity [m/s] for the whole rotor for the angular position of maximum torque coefficient (θ= 88°), N=5, λ=2.04

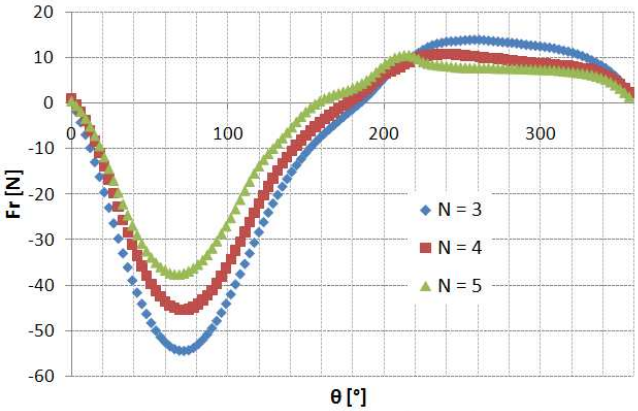

Fig. 15 Aerodynamic radial force on the blade for the tip speed ratio of peak power coefficient (the force is considered as negative if the airfoil is pushed towards the rotor axis), optimal tip speed ratio (λ=2.58 for N=3, λ=2.33 for N=4, λ=2.04 for N=5)

TABLE V
VALUES OF MAXIMUM RADIAL FORCE (ABSOLUTE VALUE) AND PERCENTILE DIFFERENCES WITH RESPECT OF N = 3

	$F_{r,\,max}$	$\Delta F_{r,max}$ [%]
N = 3	-54.5	-
N = 4	-45.5	-16.5
N = 5	-37.7	-30.8

VIII. Conclusions and Future Works

Numerical analysis were performed in order to understand the effect of blade number on the behavior of a straight-bladed vertical-axis wind turbine. The numerically predicted peak of power coefficient lowered with the increase of rotor solidity, while it moved to lower tip speed ratio. In fact, larger number

of blades allowed to reach the maximum power coefficient for lower angular velocities, but were penalized as far as efficiency is concerned.

The aerodynamic effect obtained increasing the blade number resulted similar to what occurs with the inclination of a three-dimensional blade, as discussed by Raciti Castelli et al. [2]. As can be seen from Fig. 16, the peak of the power coefficient decrease with the increment of the phase shift angle in an helical blade. Some aspect of this analogy might be further investigated. The analysis reported in [2] were made with a three-dimensional simulation of a single blade, but a complete analysis of the 3D flow would be interesting in order to see the combined effects of increase in blade number and inclination of the blade.

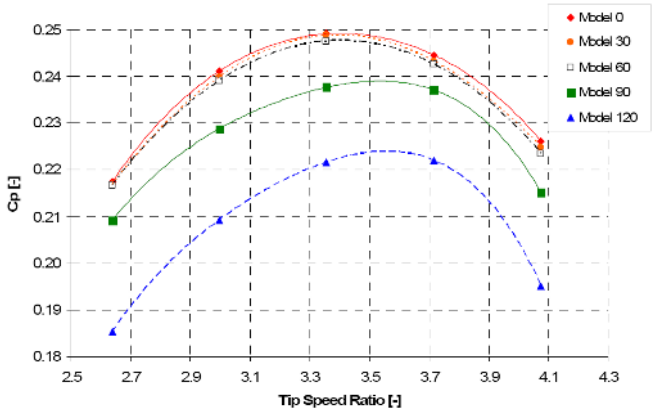

Fig. 16 Effect of phase shift angle (indicated by the numbers in the legend) on a three-dimensional vertical blade (from: [2])

Qualitatively speaking, no differences are registered in the flow field near a single airfoil in proximity of the position at which the maximum of torque coefficient happens for a single blade. This phenomenon can be due to the proximity of the tip speed ratios at which the peak of torque occurs.

With regard to the radial component of the aerodynamic forces, an increase in blade number brings to a decrease of this force, which is mush desirable from a structural perspective. Further analysis should be done to investigate the combined effect of aerodynamic radial force and centrifugal force on the structural behavior of the blade.

NOMENCLATURE

A [m^2]	rotor swept area
c [m]	chord length
C_t [-]	wind turbine torque coefficient
C_p [-]	wind turbine power coefficient
D_{rotor} [m]	Rotor diameter
F_r [N]	aerodynamic radial force
H_{rotor} [m]	rotor height
N	number of blades
P [W]	wind turbine power output
Re	Reynolds number
R_{rotor} [m]	Rotor radius
T [Nm]	wind turbine torque output
v_∞ [m/s]	free wind velocity
θ [°]	azimuthal position
λ [-]	tip speed ratio
μ [Pa·s]	dynamic viscosity
ρ [kg/m^3]	air density
σ [-]	solidity of the rotor
ω [rad/s]	rotor angular velocity

ACKNOWLEDGMENTS

The present work was developed in cooperation with Vortex Energy S.r.l. (Italy), as a part of a research project finalized to the manufacturing of a Darrieus VAWT.

REFERENCES

[1] European Wind Energy Association, EU energy policy after 2020,www.ewea.org, 2011.
[2] M. Raciti Castelli, E. Benini, Effect of blade inclination angle on a Darreius wind turbine, Journal of turbomachinery,2012.
[3] S. Li, Y. Li, Numerical study on the performance effects of solidity on the straight-bladed vertical axes wind turbine, Power and energy Engineering Conference, 2010.
[4] I.Paraschivoiu, "Wind turbine design with emphasis on Darrieus concept", Polytechnic International Press, Canada,2002.
[5] M. Dunquette, K. Visser, Numerical implications of solidity and Blade Number on Rotor Performance of horizontal-axis wind turbines, Journal of Solar Energy Engineering, November 2003.
[6] S. Ferreira, H. Bijl, G. van Bussel ,G. van Kuik, Simulating dynamic stall in a 2D VAWT: modeling strategy, verification and validation with particle image velocimetry data, The Science of making torque from wind. Journal of Physics: Conference Series 75,2007.
[7] S. Wang, Z. Tao, Numerical investigation on dynamic stall associated with low reynolds number flows over airfoils, 2nd International Conference on Computer Engineering and Technology,2010.
[8] R. Howell, N. Qin, J. Edwards, N. Durrani. Wind tunnel and numerical study of a small vertical axis wind turbine, Renewable Energy 35, 2010.
[9] J. H. Strickland: The Darrieus turbine: a performance prediction model using multiple streamtube, SAND 75e0431,1975.
[10] Fluent Inc., Fluent User's Manual,pp. 193-194, 2006.
[11] R.M. Cummings, J.R. Forsythe, S.A. Morton, K.D. Squires, Computational challenges in high angle of attack flow prediction, Prog Aerospace Sci, 2003.
[12] M. Raciti Castelli, G. Pavesi, L. Battisti, E. Benini, G. Ardizzon, Modeling strategy and numerical validation for a Darrieus vertical axis micro-wind turbine, ASME 2010 International Mechanical Engineering Congress & Exposition, Vancouver, British Columbia, Canada, November 12e18 2010.
[13] M. McMullen, A. Jameson, J.J. Alonso, Acceleration of convergence to a periodic steady state in turbomachinery flows, 39th AIAA aerospace sciences meeting & exhibit. Reno, NV: AIAA; January 8-11 2001.
[14] M. Raciti Castelli, A. Englaro, E. Benini, The Dareius wind turbine:Proposal for new performance prediction model based on CFD, Energy, Volume 36, Issue 8, August 2011.
[15] G.H. Yu, X.C. Zhu, Z.H. Du, Numerical simulation of a wind turbine airfoil: dynamic stall and comparison with experiments, Power and Energy Journal Vol. 224, 2010.